Biochimica et Biophysica Acta 1833 (2013) 2176–2189

Contents lists available at SciVerse ScienceDirect

Biochimica et Biophysica Acta

journal homepage: www.elsevier.com/locate/bbamcr

A novel actin cytoskeleton-dependent noncaveolar microdomain composed of homo-oligomeric caveolin-2 for activation of insulin signaling

Hayeong Kwon, Jaewoong Lee, Kyuho Jeong, Donghwan Jang, Yunbae Pak *

Department of Biochemistry, Division of Applied Life Science (BK21 Program), PMBBRC, Gyeongsang National University, Jinju 660-701, Republic of Korea

ARTICLE INFO

Article history:
Received 19 November 2012
Received in revised form 1 May 2013
Accepted 3 May 2013
Available online 9 May 2013

Keywords:
Caveolin-2
Insulin receptor
Actin cytoskeleton
Noncaveolar microdomain
Rab6
Microtubules

ABSTRACT

The role of caveolin-2 (cav-2), independently of caveolin-1 (cav-1) and caveolae, has remained elusive. Our data show that cav-2 exists in the plasma membrane (PM) in cells lacking cav-1 and forms homo-oligomeric complexes. Cav-2 did not interact with cavin-1 and cavin-2 in the PM. Rab6-GTP was required for the microtubule-dependent exocytic transport of cav-2 from the Golgi to the PM independently of cav-1. The cav-2-oligomerized noncaveolar microdomain was unaffected by cholesterol depletion and protected from shearing of silica-coated PM. Activation of insulin receptor (IR) was processed in the microdomain. Actin depolymerization affected the formation and sustenance of cav-2-oligomerized noncaveolar microdomain and attenuated IR recruitment to the microdomain thereby inhibiting IR signaling activation. Cav-2 shRNA stable cells and the cells ectopically expressing an oligomerization domain truncation mutant, cav-$2_{\Delta 47-86}$ exhibited retardation of IR signaling activation via the noncaveolar microdomain. Elevation in status of cav-2 expression rendered the noncaveolar activation of IR signaling in cav-1 down-regulated or/and cholesterol-depleted cells. Our findings reveal a novel homo-oligomeric cav-2 microdomain responsible for regulating activation of IR signaling in the PM.

1. Introduction

Lipid rafts are fluctuating nanoscale domains assembled with cholesterol, sphingolipid, and proteins that can be stabilized into platforms and function in membrane signaling and trafficking [1–3]. Caveolae are cav-1-enriched invaginations of the PM that represent a subdomain of the lipid rafts [4]. Cholesterol is required for the caveolae formation and maintenance [5,6]. Caveolae localization of neutral glycolipids and sphingomyelin has been shown [7,8]. Ganglioside GM1 and GM3 were enriched at lesser extent in caveolae, but also present outside caveolae [9]. GM3-enriched microdomain had different lipid composition from caveolin-enriched microdomain and was not affected by cholesterol-sequestering drugs [9,10]. Thus, these reports suggest that caveolae and sphingolipid-enriched microdomain can exist independently and that specific sphingolipids and cholesterol dependency might partition differentially between caveolae and other noncaveolar microdomains.

Although cav-1 is an essential component of caveolae, cav-1 is expressed in neurons and leukocytes lacking caveolae, and caveolins can be found outside of caveolae even in cells with caveolae [11–13]. Cav-2 in the Golgi targets to caveolae upon formation of hetero-oligomers with cav-1 [14,15] but cav-2 is not essential for caveolae formation [16–18]. Homo-oligomeric cav-1 domain in the PM, distinct from caveolae has been reported [19]. Thus numerous studies have attempted to characterize heterogeneous distribution of lipids and proteins between caveolae and noncaveolar microdomains. Nevertheless, specificity for transmembrane signal activation through PM microdomains is restricted to caveolae because of lack of visibility as morphological structures and information for the dynamic formation of the noncaveolar microdomains.

Our investigation of cav-2 regulation of insulin signaling, independently of cav-1 and caveolae, in cells lacking cav-1 and cav-2-expressed cells having no endogenous caveolins showed that cav-2 interacts with IR and activates IR signaling [20–24]. Although cav-2 targeting to caveolae in PM was known to depend on cav-1 [14,15,18,25–27], our studies using subcellular fractionation and PM sheet assay indicated that cav-2 localizes in the PM in the absence of cav-1. The cav-2 localization was unaffected by cholesterol depletion and its level was not changed in response to insulin [28]. Further, our studies demonstrated that cav-2 but not cav-1 translocates to the nucleus specifically in response to insulin [20–24,28]. Our investigation on subcellular distribution of cav-2 and cav-2 pool responsible for the nuclear targeting showed that cav-2 in the Golgi, but not PM is transported to the inner nuclear membrane in response to insulin [28]. Thus the findings suggest that cav-2 pool in the PM is distinct from those in the Golgi and nucleus and might have different physiochemical property and function irrespectively of cav-1. However, even though cav-2 would presumably

Abbreviations: Cav-2, caveolin-2; Cav-1, caveolin-1; IR, insulin receptor; PM, plasma membrane; HLDM, heavy low-density insoluble membrane; LLDM, light low-density insoluble membrane; GPMV, giant plasma membrane vesicle; LDMV, low density membrane vesicle; CTB, cholera toxin B subunit; MβCD, methyl-β-cyclodextrin; CCD, cytochalasin D; LatB, latrunculin B; TfR, transferrin receptor

* Corresponding author. Tel.: +82 557721354; fax: +82 557599363.
E-mail address: ybpak@nongae.gsnu.ac.kr (Y. Pak).

0167-4889/$ – see front matter © 2013 Elsevier B.V. All rights reserved.
http://dx.doi.org/10.1016/j.bbamcr.2013.05.003

interact with IR in the PM in the absence of cav-1, molecular mechanism of PM targeting of cav-2 and its functional significance in the PM have not been explored.

Here, we report that a novel actin cytoskeleton-dependent cav-2-enriched noncaveolar microdomain regulates IR signaling in the PM. Further, our data demonstrate that elevation of cav-2 expression status relative to cav-1 leads to reconstitution of the noncaveolar microdomain for activation of IR signaling in caveolae-depleted cells.

2. Materials and methods

2.1. Materials

Antibodies and reagents used were purchased as follows: anti-cav-2 (BD 610685), anti-cav-1 (BD 610406), anti-flotillin-1 (BD 610820), anti-ERK1 (BD 610031), anti-Akt (BD 610860), anti-phosphotyrosine-PY20 (BD 610000), and E-cadherin (BD 610182) antibodies from BD Transduction Laboratories; anti-GM130 (ab31561) antibody from Abcam; anti-calnexin (sc-11397), anti-IR (sc-711), anti-cav-2 (sc-7942), and anti-actin (sc-1616) antibodies from Santa Cruz Biotechnology; anti-GFP (#2555), anti-p-ERK (#9101), and anti-p-Akt (#9271) antibodies form Cell Signaling; anti-FLAG® M2 (F 1804), anti-rabbit IgG-peroxidase (A 6154), and anti-mouse IgG-peroxidase conjugate (A 4416) antibodies from Sigma-Aldrich; anti-transferrin receptor (TfR) (13-6800) antibody from Invitrogen; cholera toxin B subunit (CTB)-Alexa Fluor® 594 conjugates (C-34777) from Molecular Probes; human insulin from Eli Lilly; colchicine (C3915), methyl-β-cyclodextrin (MβCD) (C4555), cytochalasin D (CCD) (C8273), and 4′-6-Diamidino-2-phenylindole (DAPI) (D8417) from Sigma-Aldrich; U18666A (662015) and latrunculin B (LatB) (428020) from Calbiochem.

2.2. Cell culture

Hirc-B cells were maintained in Dulbecco's modified Eagle's medium (DMEM) (Gibco/BRL, Grand Island, NY) containing 5 mM D-glucose supplemented with 10% (v/v) fetal bovine serum (FBS) (Sigma, St. Louis, MO), 100 nM methotrexate (Sigma, St. Louis, MO), and 0.5% gentamycin (Gibco/BRL, Grand Island, NY) in a 5% CO_2 incubator at 37 °C. HEK293T and 3T3L1 cells were grown in DMEM containing 5 mM D-glucose supplemented with 10% (v/v) FBS and 0.5% penicillin/streptomycin (Sigma, St. Louis, MO) in a 5% CO_2 incubator at 37 °C.

2.3. Plasmids

A full-length cav-2 (GenBank Accession No. NM_131914) [21–24,28], Rab6 (NM_002869) [28], cavin-1 (NM_012232.5), cavin-2 (NM_004657.5), or flotillin-1 (NM_005803) cDNA was subcloned into pcDNA3 vector (Invitrogen, Carlsbad, CA). The resulting entry vector of cav-2, cavin-1, cavin-2, or flotillin-1 was converted into self-constructed GFP tagging destination expression vector (pEGFP-N1 vector, Clontech Laboratories). IR (NM_10051.1) plasmid (Gateway PLUS shuttle clone for INSR, GC-Y2826-CF) was obtained from Genecopoeia. For construction of a vector expressing mCherry or FLAG-tagged cav-2 or GFP-tagged IR, cav-2 or IR was subcloned into the pDonor207 and then moved into the pDEST-N-RFP, pDS_FLAG-XB or pDS_GFP-XB vector using Gateway™ Technology (Invitrogen). DsRed-Monomer was replaced with mCherry in order to improve fluorescence intensity. FLAG-cav-$2_{\Delta 47-86}$ mutant was generated by using FLAG-cav-2 as template via EZchange site-directed mutagenesis kit (Enzynomics, Daejeon, Korea). A construct encoding T27N-Rab6 was generated by PCR mutagenesis using mutated oligonucleotides as described [28]. All expression vectors were verified by sequencing.

2.4. Reverse transcription-PCR

Total RNA was extracted from Hirc-B and HEK293T cells with TRIzole reagent (SolGent Co., Ltd.). cDNA was generated using reverse transcription kit (Bioneer). The cDNA was used as the template for the subsequent PCR amplification. PCR primers were for glyceraldehydes-3-phosphate dehydrogenase (GAPDH); 5′-ACCACCATGGAGAAGGCTGG-3′ and 5′-CTCAGTGTAGCCCAGGATGCC-3′, cav-2 (rat); 5′-ATGGGGCTGGAGACTGAGAAG-3′ and 5′-TCAGTCATGGCTCAGTTGCATG-3′, cav-2 (human); 5′-ATGGGGCTGGAGACGGAG-3′ and 5′-TCAATCCTGGCTCAGTTGCA-3′, cav-1 (rat); 5′-ATGTCTGGGGGTAAATACGTA-3′ and 5′-TCATATCTCTTTCTGCGTGCT-3′, cav-1 (human); 5′-ATGTCCACGGGCGGAGACTTC-3′ and 5′-TTATATTTCTTTCTGCAAGTTGATGCG-3′. PCR was performed using AccuPower PCR PreMix kit (Bioneer). The PCR fragments were separated by running on 1% agarose gels.

2.5. Ablation of endogenous cav-2 by shRNA

To establish stable cell lines that express a cav-2 short-hairpin RNA (shRNA), a cav-2 specific shRNA lentiviral plasmid set (MISSION®shRNA Bacterial Glycerol Stock) and the MISSION® Non-Target shRNA Control Vector (pLKO.1-puro) were purchased from Sigma. For stable transfection, Hirc-B cells were transfected with cav-2 shRNA expressing plasmid. After 48 h incubation, 1 μg/ml puromycin (Clontech, USA) was added to the cultures to select for puromycin-resistant clones. One week later, independent colonies were picked using cloning cylinder (Sigma, St. Louis, MO), subcultured, and tested for cav-2 expression by RT-PCR and immunoblot analysis. Stable cell lines that express a cav-2 shRNA were then selected.

2.6. Silencing of Rab6, cav-1 and cav-2 by siRNA

siRNA targets of Rab6, cav-1, cav-2, and scramble control were purchased from Bioneer Corp. (Daejon, Korea) and Dharmacon Research, Inc., respectively. The siRNA oligonucleotides were synthesized to the following target sequences: Rab6; sense (5′-AGGCAGAUCAGGUAAAGCA-3′) and antisense (5′-UGCUUUACCUGAUCUGCCU-3′), cav-1; sense (5′-CAGUUGUACCAUGCAUUAA-3′) and antisense (5′-UUAAUGCAUGGUACAACUG-3′), cav-2; sense (5′-GUAAAGACCUGCCUAAUGGUU-3′) and antisense (5′-PCCAUUAGGCAGGUCUUUACUU-3′, scramble control; 5′-GGAAAGACUGUUCCAAAAA-3′. Transfection of the siRNA duplexes was carried out using DharmaFECT Transfection Reagents (Dharmacon) for 48 h.

2.7. Confocal microscopy

Hirc-B cells were fixed with 3.7% paraformaldehyde in phosphate-buffered saline (PBS) for 20 min, and permeabilized with 0.1% Triton X-100 in PBS for 20 min. Permeabilized cells were rinsed with PBS and blocked with 1% bovine serum albumin (BSA) in PBS for 1 h at room temperature (RT). Cells were rinsed with PBS and incubated with anti-cav-2 and anti-IR antibodies in 1% BSA in PBS for overnight at 4 °C. After washing three times with PBS, the cav-2 and anti-IR antibodies were detected with TRITC- and FITC-conjugated anti-mouse and anti-rabbit secondary antibodies, respectively in 1% BSA in PBS for 2 h at RT. The coverslips were washed and mounted on glass slides. Fluorescent images were obtained using an Olympus Fluoview 1000 confocal microscope attached to an Olympus BX61 vertical microscope equipped with PlanApo 60×/1.40 oil immersion objective (Olympus). Quantitation of colocalization of cav-2 with IR was performed with the Line Profile Tool of Image-ProPlus 6.1 (Media Cybernetics). To analyze colocalization of cav-2 with cavin-1 or cavin-2, cavin-1-GFP or cavin-2-GFP transfected Hirc-B cells were subjected to confocal microscopy analysis using anti-cav-2 primary and anti-TRITC-conjugated anti-mouse secondary antibodies as above.

2.8. Subcellular fractionation

Subcellular fractionation was carried out to generate the fractions that are enriched in markers of the PM, ER (high density microsomes, HDM), and Golgi (low density microsomes, LDM) as described previously [29,30]. Briefly, cells were washed with ice-cold PBS and scraped into isotonic buffer containing 250 mM sucrose, 20 mM Tris–HCl, 1 mM EDTA, 15 mM KCl, 2 mM $MgCl_2$, 1 mM phenylmethylsulfonyl fluoride (PMSF), 1 mM sodium orthovanadate, 1 μg/μl aprotinin, and 1 μg/μl leupeptin. Cell lysates were homogenized using 10 strokes of a Dounce homogenizer and centrifuged at 10,000 ×*g* for 45 min at 4 °C. The membrane pellet was resuspended in the isotonic buffer. The PM was isolated by loading the resuspended membrane pellet onto a 1.12 M sucrose cushion and centrifuging at 100,000 ×*g* for 2 h at 4 °C in a SW41Ti rotor (Beckman Instruments). The PM fraction at the interface was collected, diluted with ice-cold PBS and pelleted by centrifugation at 200,000 ×*g* for 1 h at 4 °C in a SW41Ti rotor. The initial supernatant was centrifuged at 48,000 ×*g* for 20 min at 4 °C in TLA-100.3 rotor (Beckman Instruments), yielding a pellet of HDM. The supernatant was then recentrifuged at 212,000 ×*g* for 70 min at 4 °C in TLA-100.3 rotor, yielding a pellet of LDM.

2.9. Cell surface biotinylation assay

Cell surface proteins were biotinylated with the membrane-impermeant reagent sulfo-NHS-LC-biotin (0.5 mg/ml) in PBS containing 0.1 mM $CaCl_2$ and 1 mM $MgCl_2$ for 45 min at 4 °C. Cells were washed with ice-cold PBS and lysed with lysis buffer (50 mM Tris–HCl, 1 mM EDTA, 150 mM NaCl, 10% glycerol, 1% Nonidet P-40, and protease inhibitor, pH 7.4). Biotinylated proteins were precipitated with NeutrAvidin agarose bead (Pierce) for 2 h at 4 °C while shaking. The immunocomplexes were collected by centrifugation at 12,000 rpm for 10 min at 4 °C and washed twice with lysis buffer and twice with PBS. After the final wash the pellet was resuspended in 30 μl of 2× SDS-PAGE sample buffer. The immunoprecipitates were then resolved, separated by SDS-PAGE, and subjected to immunoblot analysis.

2.10. PM sheet assay

PM sheet assay was performed as described previously [28]. Briefly, cav-2-GFP-transfected Hirc-B cells were incubated on ice with 0.5 mg/ml of poly-L-lysine in PBS for 30 s and washed with ice-cold hypotonic buffer (23 mM KCl, 10 mM Hepes, pH 7.5, 2 mM $MgCl_2$, and 1 mM EGTA). The cells were sonicated for 3 s (Sonics Vibra Cell Sonicator, set at 10% amplitude) in ice-cold sonication buffer (70 mM KCl, 30 mM Hepes, pH 7.5, 5 mM $MgCl_2$, 3 mM EGTA, 1 mM DTT, and 0.1 mM PMSF) and used for confocal microscopy analysis. To assess colocalization of cav-2-GFP with endogenous IR or cav-2 and cav-2 with TfR or flotillin-1, PM sheet images were analyzed using Intensity Correlation Analysis Plugin of the Image J [31]. The distribution of the intensity value for each pixel of a channel is plotted against the product of the difference of the mean (PDM) of the two channels. The PDM value is expressed as "PDM = (green intensity − mean green intensity) × (red intensity − mean red intensity)". The PDM image where each pixel is equal to the PDM value at that location is pseudocolored in yellow and the areas in blue represent the areas of positive and negative PDM values, corresponding to the presence and absence of colocalization, respectively.

2.11. Electron microscopy

For immunoelectron microscopy, Hirc-B cells were rinsed and incubated at 37 °C in Ringer's solution for 15 min before being fixed in Ringer's solution containing 2% paraformaldehyde and 0.2% glutaraldehyde for 30 min at 37 °C. The fixed cells were rinsed in PBS, scraped and collected by centrifugation. The cell pellet was postfixed for 30 min with 1% osmium tetroxide (O_sO_4) in PBS containing 1.5% potassium ferrocyanide (reduced osmium), dehydrated, and embedded in LR-White resin as previously described [32]. Ultrathin sections mounted on formvar-coated nickel grids were blocked with 3% BSA in PBS for 30 min, and then incubated with anti-cav-2 antibody for 1 h followed by 18 nm gold-conjugated goat anti-rabbit antibody (Jackson Immuno Research Laboratories, Inc.) for 1 h. The sections were then stained with 2% uranyl acetate and examined in a Tecnal 12 transmission electron microscope (FEI Co., Hillsboro, OR). For electron microscopy, cells were fixed with 2.5% glutaraldehyde for 2 h, postfixed with 1% O_sO_4 for 2 h, dehydrated, and embedded in LR-White resin. Ultrathin sections were placed on copper grids, poststained with 2% (w/v) aqueous uranyl acetate and lead citrate, and then observed by electron microscope.

2.12. Velocity gradient centrifugation

Sucrose velocity gradient centrifugation was performed as described previously [33,34]. 3T3L1 and Hirc-B cells were lysed in 0.5, 1 or 2% TX-100, or in 60 or 120 mM n-octylglucoside (OG) lysis buffer (100 mM NaCl, 20 mM Tris–HCl, pH 7.4, 5 mM EDTA, and protease inhibitors) for 20 min at RT. The lysates were centrifugated at 1100 ×*g* for 5 min. The supernatant was loaded onto 10–40% linear sucrose gradients containing 0.5, 1 or 2% TX-100, or in 60 or 120 mM OG lysis buffer. After centrifugation in a SW41Ti rotor at 237,020 ×*g* for 255 min at 4 °C, fourteen 720 μl fractions were collected from the top to the bottom. An equal volume from each gradient fraction was separated by SDS-polyacrylamide gel electrophoresis (PAGE) and subjected to immunoblot analysis.

2.13. Quantitation of cholesterol

Cholesterol was measured by using an Amplex® Red Cholesterol Assay Kit (Molecular Probes, A12216) according to the manufacturer's protocols.

2.14. Isolation of low-density membrane vesicle (LDMV) from silica-coated PM

Isolation of PM using cationic silica (LUDOX® CL colloidal silica (Sigma-Aldrich, 420883)) was performed as described previously [35]. 3T3L1, Hirc-B, and HEK293T cells were washed with ice-cold PBS and scraped into 2 ml PM coating buffer (PMCB: 20 mM MES, 150 mM NaCl, and 800 mM sorbitol, pH 5.3) and placed into a 5 ml 10% suspension of cationic colloidal silica in PMCB drop by drop. The solution was shaken gently at 4 °C for 15 min and added with 20 ml PMCB, and centrifuged at 900 ×*g* for 5 min at 4 °C. The pellet was washed with 20 ml PMCB and centrifuged at 900 ×*g* for 5 min at 4 °C to remove any excess silica. The cells were suspended in 2 ml PMCB and placed dropwise into a buffer of 10 mg/ml polyacrylicacid in PMCB. The solution was rocked and centrifuged at

Fig. 1. Cav-2 colocalizes with IR in the PM. (A) Hirc-B cells were labeled with anti-cav-2 and anti-IR antibodies followed by TRITC- and FITC-conjugated antibodies. DNA was stained using DAPI. HEK293T cells were cotransfected with cav-2-mCherry and IR-GFP. Scale bar, 20 μm. (B) Cav-1 and cav-2 mRNA levels were analyzed by RT-PCR. GAPDH was coamplified as the internal control. (*r*, rat; *h*, human) (C) Hirc-B cells were processed for immunogold staining. Arrows in the left and middle panels indicate localization of gold-labeled cav-2 in the PM. Right panel shows a representative electron microscope exhibiting the absence of caveolae. (*PM*, plasma membrane; *G*, Golgi; *N*, nucleus; *M*, mitochondria) Scale bars, 0.2 μm. (D) Hirc-B and cav-2-transfected HEK293T cells were fractionated and analyzed by immunoblotting using antibodies against cav-2, or IR and detected with antibodies specific for E-cadherin, calnexin and GM130 as makers for the PM, HDM (ER) and LDM (Golgi) fractions. (E) Hirc-B and cav-2-transfected HEK293T cells were labeled with sulfo-NHS-LC-biotin and cell surface biotinylation was assayed. (F) Colocalization of cav-2-GFP with endogenous IR or cav-2 and cav-2 with TfR in the PM sheets derived from Hirc-B cells is shown in Merge and PDM values. (yellow, positive PDM; blue, negative PDM) Scale bars, 20 μm.

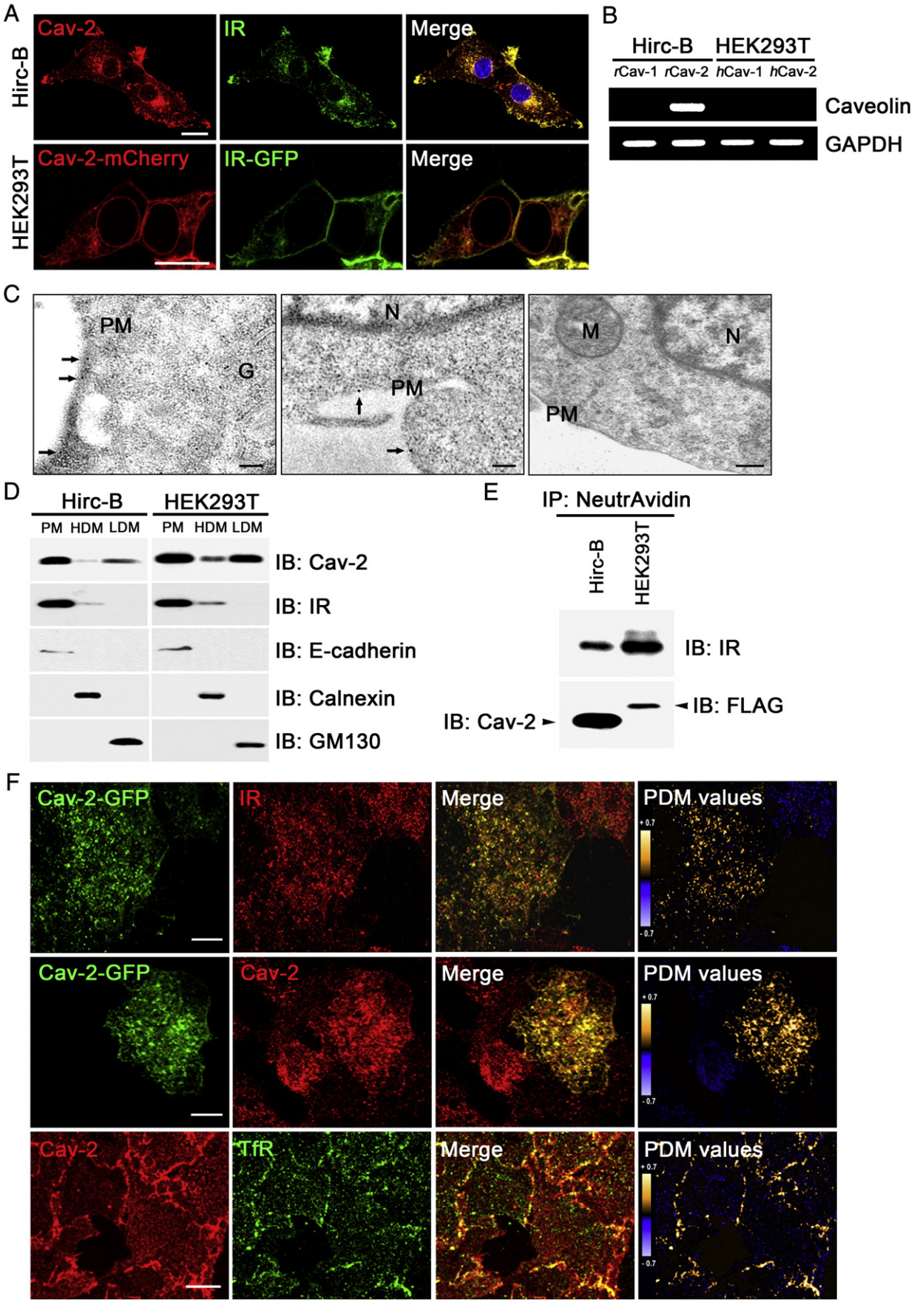
A
Hirc-B
Cav-2
IR
Merge
HEK293T
Cav-2-mCherry
IR-GFP
Merge
B
Hirc-B
HEK293T
rCav-1 rCav-2 hCav-1 hCav-2
Caveolin
GAPDH
C
PM
G
N
PM
M
N
PM
D
Hirc-B
HEK293T
PM HDM LDM
PM HDM LDM
IB: Cav-2
IB: IR
IB: E-cadherin
IB: Calnexin
IB: GM130
E
IP: NeutrAvidin
Hirc-B
HEK293T
IB: IR
IB: Cav-2
IB: FLAG
F
Cav-2-GFP
IR
Merge
PDM values
+0.7
-0.7
Cav-2-GFP
Cav-2
Merge
PDM values
Cav-2
TfR
Merge
PDM values

900 ×g for 5 min at 4 °C. The pellet was resuspended in 2 ml ice-clod hypotonic lysis buffer (2.5 mM imidazole, pH 7.0, and 1 mM PMSF) on ice for 30 min with interval vortex, and was broken with 50 strokes by a tight-fitting Dounce homogenizer. The lysates were centrifuged at 900 ×g for 20 min at 4 °C. The pellet including the nuclei and silica-coated PM was resuspended in 10% sucrose solution. Four ml of 69% sucrose was placed at the bottom of an ultracentrifuge tube and a discontinuous sucrose gradient was generated by layering 4 ml of 54% sucrose, and then 4 ml of the 10% sucrose solution including nuclei and silica-coated PM. Gradients were centrifuged at 30,000 ×g for 2 h at 4 °C in a SW41Ti rotor. The cationic silica-coated PM fraction at the bottom of the tube was resuspended in hypotonic lysis buffer and centrifuged at 30,000 ×g for 20 min at 4 °C in a SW41Ti rotor. LDMVs were separated from the silica-coated PM by sonication and then LDMV fractions were isolated by ultracentrifugation in the discontinuous sucrose gradient system as described [36].

2.15. Extraction of lipid microdomains from PM fractions

To separate HLDM from LLDM in the PM, the purified PM fractions from the subcellular fractionation as described above were subjected to a four-step sucrose density gradient fractionation as described [37,38]. Briefly, purified PM was resuspended with 2 ml of 500 mM sodium carbonate, pH 11.0 and homogenized using 10 strokes of a Dounce homogenizer, and mixed with 2 ml of 90% sucrose in Mes-buffered saline (MBS: 25 mM MES, 150 mM NaCl, pH 6.5). The extraction mixture was placed at the bottom of an ultracentrifuge tube and overlaid with 3 ml of 35% sucrose, 4 ml of 21% sucrose, and 1 ml of 5% sucrose in MBS containing 250 mM sodium carbonate. Gradients were centrifuged at 280,000 ×g for 18 h at 4 °C in a SW41Ti rotor. From the top of each gradient, 0.5 ml gradient fractions were collected to yield a total of 24 fractions. An equal volume from each gradient fraction was separated by SDS-PAGE and subjected to immunoblot analysis.

2.16. Giant plasma membrane vesicle (GPMV) isolation

Isolation of GPMVs was performed as described [39]. Briefly, Hirc-B cells were grown to confluency in a 25 cm^2 tissue culture flask and co-transfected with cav-2-mCherry and flotillin-1-GFP. Cells were then treated with or without 10 mM MβCD for 2 h, 1 μM CCD for 15 min, or 1 μM LatB for 30 min. Cells were washed twice with GPMV buffer (2 mM $CaCl_2$, 10 mM Hepes, and 0.15 M NaCl, pH 7.4), and ~1.5 ml of freshly prepared GPMV reagent was added, consisting of 2 mM N-ethylmaleimide in GPMV buffer. The flasks were incubated for 1 h at 37 °C while slowly shaking at 60 rpm. After incubation, GPMVs that had detached from the cells were gently decanted into a conical tube. The tube was allowed GPMVs to settle on ice for 45 min and the GPMVs were collected by removing ~20% of the total volume from the bottom of the tube. For making microscopy samples, a chamber was created by a square of vacuum grease (Dow Corning) on a coverslip, into the middle of which 20 μl of GPMV suspension was deposited, followed by sealing of the chamber with another coverslip. The fluorescence of the GPMVs was visualized using a confocal microscope system (BX-61; Olympus) equipped with a PlanApo 100×/1.35 oil immersion objective lens (Olympus). For microscopic analysis of cav-2 localization in ganglioside-enriched LLDM, GPMVs were incubated with 2 μg/ml of CTB-Alexa Fluor® 594 conjugates for 30 min at 4 °C before making microscopy samples. Measurement of colocalization of cav-2-GFP with CTB-Alexa Fluor® 594 conjugates or cav-2-mCherry with flotillin-1-GFP was performed by the Colocalization Finder Plugin of Image J as described previously [24,28]. The amount of colocalization of cav-2-GFP with CTB-Alexa Fluor® 594 conjugates or cav-2-mCherry with flotillin-1-GFP was calculated as the number of colocalized pixels with threshold pixels in the CTB-Alexa Fluor® 594 conjugates or flotillin-1-GFP. Averages and standard errors were computed over five images per condition for a minimum of twenty GPMVs per condition ($n = 3$).

2.17. Dot blot

For analysis of ganglioside GM1, equal volume of the fractionated samples from the four-step sucrose density gradient fractionation of the PM as described above was dot-blotted onto Hybond-C extra nitrocellulose membranes (Amersham Pharmacia Biotech). The membranes were blocked with 5% (v/v) nonfat dry milk in TBS, 0.1% (v/v) Tween 20 and incubated with HRP-conjugated CTB (Invitrogen, Molecular Probes, C-34780), a ligand for ganglioside GM1 in the PM, and then revealed by chemiluminescence.

2.18. Immunoblotting

An equal volume from each gradient fraction was separated by SDS-PAGE and transferred to a polyvinylidenedifluoride membrane (Millipore). The membrane was blocked overnight at 4 °C with 5% non-fat dry milk in TBS, 0.1% (v/v) Tween 20 and then incubated with primary antibody for 2 h at RT. After washed with TBS, 0.1% (v/v) Tween 20, the membrane was incubated with peroxidase-conjugated secondary antibody for 1 h at RT. The membrane was washed with TBS, 0.1% (v/v) Tween 20 and the blot was developed using the ECL detection reagent (RPN2106, Amersham Biosciences).

2.19. Immunoprecipitation

HEK293T cells were cotransfected with cavin-1-GFP or cavin-2-GFP and FLAG-cav-2 and subjected to the PM fractionation as described above. The purified PM pellet was resuspended in immunoprecipitation buffer (1% Triton X-100, 150 mM NaCl, 10 mM Tris–HCl (pH 7.4), 1 mM EDTA, 1 mM EGTA (pH 8.0), 0.2 mM sodium orthovanadate, 0.2 mM PMSF, and 0.5% Nonidet P-40) containing 60 mM OG and incubated overnight with anti-FLAG antibody at 4 °C. Then 20 μl of protein G-Agarose (Calbiochem) was added and the mixture was rotated for 4 h at 4 °C. The immunocomplexes were collected by centrifugation at 12,000 rpm for 10 min at 4 °C and washed three times with ice-cold immunoprecipitation buffer. After the final wash the pellet was resuspended in 30 μl of 2× SDS-PAGE sample buffer. The immunoprecipitates were then resolved, separated by SDS-PAGE, and subjected to immunoblot analysis. For immunoprecipitation analysis of IR with cav-2, Hirc-B cells were pretreated with or without 1 μM CCD for 15 min or 1 μM LatB for 30 min followed by incubation with or without 100 nM insulin for 10 min, washed with ice-cold PBS and lysed in the immunoprecipitation buffer containing 60 mM OG. The lysates were centrifugated at 12,000 rpm for 20 min at 4 °C and the supernatants were subjected to immunoprecipitation with anti-IR antibody and analyzed as described above.

2.20. Statistics

Chemiluminescent images of immunoblots were analyzed by scanning densitometry using a Kodak Gel Logic 100 imaging System (Eastman Kodak Co., New Haven, CT, USA). Data were analyzed with Student's t test. Values are given as means ± S.E. P values of < 0.05 were indicated in figures. Unless otherwise stated, n refers to independent experiments, each performed in triplicate.

3. Results

3.1. Cav-2 colocalization with IR in the PM

Being consistent with the intracellular distribution of cav-2 from our recent report [28], cav-2 localization in the Golgi, ER, inner

nuclear membrane, and PM is detected by confocal immunofluorescence microscopy in Hirc-B cells expressing cav-2 without cav-1 and cav-2-transfected HEK293T cells with no detectable endogenous cav-1 and cav-2 expression (Fig. 1A). No cav-1 expression in the cells is demonstrated by RT-PCR analysis (Fig. 1B). The localization of cav-2 in the PM (Fig. 1C, *Arrows*) and Golgi is further demonstrated by immunoelectron microscopy. As we have also previously demonstrated that cav-2 prolongs IR activation by its interaction with IR [23], endogenous cav-2 colocalizes with IR in the PM in Hirc-B cells (Fig. 1A, top panel). And when HEK293T cells were cotransfected with cav-2-mCherry and IR-GFP, cav-2-mCherry comerged with IR-GFP in the PM (Fig. 1A, bottom panel). Subcellular fractionation confirmed the subcellular localization of cav-2 observed by confocal microscopy (Fig. 1A) and demonstrated that cav-2 is cofractionated in the PM fraction with IR in Hirc-B cells and cav-2-expressed HEK293T cells (Fig. 1D). To further verify if cav-2 interacts with IR in the PM, cell surface biotinylation assay was performed. As shown in Fig. 1E, cav-2 was in association with the cell surface biotinylated IR. PM sheet assay with a detailed quantitative colocalization analysis also confirmed that cav-2 colocalizes with IR in the PM (Fig. 1F, top panel). This is demonstrated in a false color image (PDM values); yellow color represents dependent localization of both factors, whereas blue color shows segregated localization. The cav-2-GFP comerged with endogenous cav-2 in the PM sheets (Fig. 1F, middle panel) but cav-2 did not colocalize with TfR, a non lipid-rafts PM marker protein (Fig. 1F, bottom panel). Together, these data demonstrate that cav-2 colocalizes with IR in the PM and point out that cav-2 localizes in the PM independently of cav-1.

3.2. Microtubule-dependent Rab6-GTP-mediated PM targeting of cav-2

Rab6 regulates exocytic transport by enhancing kinesin-driven movement of secretory vesicle from the Golgi [40]. We have previously demonstrated that cav-2 specifically interacts with Rab6 [28]. Thus, we explored whether the PM targeting of cav-2 is regulated by the Rab6-dependent transport. In the PM sheet derived from Hirc-B cells, cav-2-GFP colocalized with flotillin-1, a lipid-rafts PM marker protein (Fig. 2A, top panel). However, cav-2-GFP was not detected in the PM sheet derived from Rab6-depleted cells indicating complete inhibition of cav-2 targeting to the PM (Fig. 2A, bottom panel). When cells were transfected with dominant negative T27N-Rab6 mutant, endogenous cav-2 targeting to the PM was greatly reduced as compared to vector control (Fig. 2B). To further test whether the translocation of cav-2 to the PM is dependent on microtubule-based transport, cells were treated with colchicine, a microtubule depolymerization agent. In untreated cells, endogenous cav-2 comerged with flotillin-1 (Fig. 2C, top panel). However, the colocalization was inhibited in the PM sheet from the colchicine-treated cells (Fig. 2C, bottom panel). Analysis of PDM values verified requirement of Rab6-GTP and microtubules in the PM targeting of cav-2.

3.3. Noncaveolar homo-oligomeric cav-2 microdomain refractory to the cholesterol depletion in the PM

To examine whether cav-2 exists as oligomerized form, sucrose velocity gradient centrifugation was performed. Cav-2 formed large hetero-oligomeric complexes (fractions, 8–11; high MW) with cav-1 (*i.e.* the 70S oligomers [33]) in 3T3L1 cells (Fig. 3A, a). To assess integrity of the oligomeric complexes, we tested effects of detergents, 60 and 120 mM OG on the solubilization of the complexes prior to sucrose velocity gradient centrifugation. The hetero-oligomers were resolved in monomeric and small oligomeric complexes (fractions, 1–4; low MW) (*i.e.* the 8S oligomers [33]) by 60 and 120 mM OG treatments. In Hirc-B cells, cav-2 formed large homo-oligomeric complexes (fractions, 8–11; high MW) without cav-1 (Fig. 3A, b). The homo-oligomers were resolved in monomeric and small oligomeric complexes (fractions, 1–4; low MW) by 2% TX-100 and 60 and 120 mM OG but not by 0.5 and 1% TX-100 treatments. Oligomer formation of cav-2 was observed in the non-boiled and 60 mM OG-treated non-boiled, consistent with the result shown in Fig. 3A, b, samples but not detected in the boiled and 120 mM OG-treated non-boiled samples (Fig. 3A, c). Thus, these results show that cav-2 without cav-1 is able to form large homo-oligomeric complexes in the PM. Either MβCD treatment to deplete cholesterol from the PM (70–85% depletion) or U18666A treatment from the Golgi complex [41] (~50% depletion) did not affect the formation of cav-2 oligomeric complexes (Fig. 3B).

As we explored structural feature of cav-2-localized microdomain by analyzing isolated LDMV by shearing of silica-coated PM (Fig. 3C), cav-2 was detected with cav-1 in the LDMV (fractions, 4–6) in the PM of 3T3L1 cells having caveolae [42], and protected from the shearing indicating that hetero-oligomerized cav-1/cav-2 formed invaginated caveolae. When caveolae were disrupted by MβCD treatment, cav-2 was no longer detected with cav-1 in the LDMV fraction. In Hirc-B and cav-2-expressed HEK293T cells lacking cav-1, cav-2 was also protected from the shearing and detected in the LDMV but the cav-2 in the LDMV was unaffected by MβCD treatment (Fig. 3C). Being consistent with the observation from the electron microscope image of Hirc-B cells exhibiting the absence of caveolae (Fig. 1C, right panel), cav-2 did not interact with cavin-1 and cavin-2 known as regulators of caveolae biogenesis [43] in the PM (Fig. 3D, a). Confocal microscopy analysis also confirmed that cavin-1-GFP or cavin-2-GFP does not colocalize with cav-2 in the PM (Fig. 3D, b). These results identify a noncaveolar microdomain composed of homo-oligomerized cav-2 in the PM and show that the microdomain has a unique structure that is protected from shearing of silica-coated PM and distinct from cholesterol-dependent microdomain.

3.4. Actin cytoskeleton-dependent formation of homo-oligomeric cav-2 microdomain for insulin signaling activation via IR recruitment

To characterize cav-2-enriched noncaveolar microdomain in the PM, a four-step sucrose density gradient fractionation was performed to separate light low-density insoluble membrane (LLDM) and heavy low-density insoluble membrane (HLDM) with purified PM. As shown in Fig. 4A, ganglioside GM1 was enriched in the LLDM (fractions, 1–4) and flotillin-1 in the HLDM (fractions, 9–12) in control as previously demonstrated [37,38]. Cav-2 was detected in the HLDM and the localization was unchanged in response to insulin. IR also localized in the HLDM where IR signaling was activated by insulin stimulation (Fig. 4A, a and b). Cholesterol was enriched in the HLDM of the PM and was depleted by MβCD treatment (Fig. 4A, c). The colocalization of cav-2 and IR was refractory to the cholesterol depletion and activation of IR, ERK and Akt was transduced in the HLDM in response to insulin (Fig. 4A, d). These results show that IR signaling is activated in the noncaveolar cav-2 and IR-colocalized HLDM with no requirement of cholesterol.

Actin cytoskeleton participates in regulating lipid rafts-associated signaling events [44–46]. To explore if actin cytoskeleton is involved in localization of cav-2 and activation of IR signaling in the HLDM, Hirc-B cells were treated with CCD or LatB. Depolymerization of actin affected cav-2 localization in the HLDM and led to the detection of cav-2 in the LLDM. And activation of IR signaling was not processed in the HLDM although IR was detected in the HLDM (Fig. 4A, e and f). To examine whether cav-2 regulates insulin signaling via IR recruitment to the HLDM, IR protein level associated in the HLDM fraction relative to that in whole cell lysate (WCL) was determined by resolving equal amounts of protein from WCL and LLDM and HLDM fractions on SDS-PAGE and immunoblot analysis (Fig. 4B). Levels of cav-2 and IR, and tyrosine phosphorylation of IR were elevated in the HLDM fraction relative to WCL (Fig. 4B, lanes 1 vs. 3). And ERK and Akt were also detected and activated in the HLDM. LatB

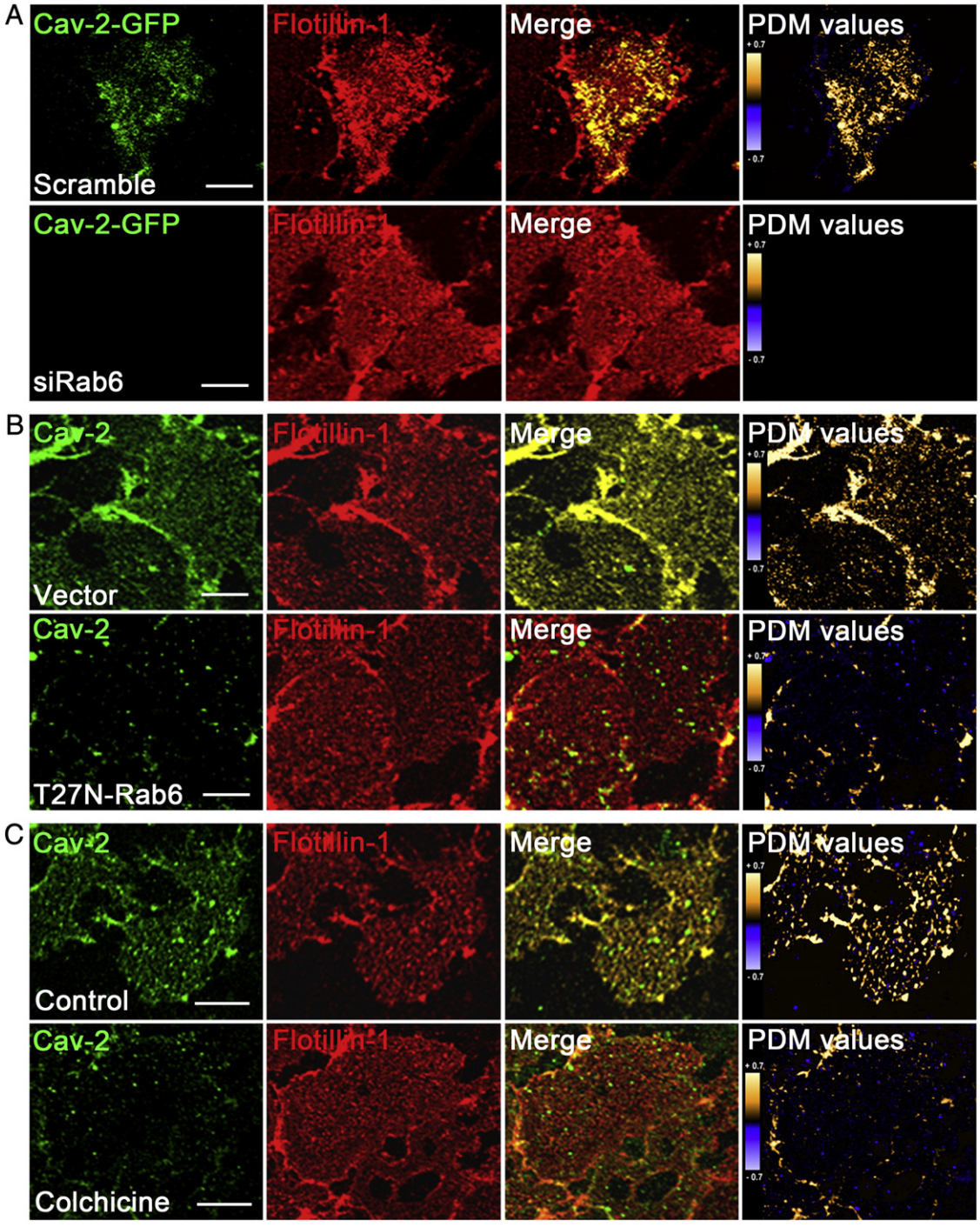

Fig. 2. PM targeting of cav-2 is blocked by Rab6 siRNA, dominant negative T27N-Rab6 mutant, and colchicine treatment. Hirc-B cells were transfected with cav-2-GFP and scramble control or siRab6 (A), T27N-Rab6-mCherry (B), or treated with or without 10 μM colchicine for 3 h (C). PM sheets were prepared from the cells and stained with antibodies against cav-2 and flotillin-1. Colocalization of cav-2-GFP or cav-2 with flotillin-1 in the PM sheets is shown in Merge and PDM values. (yellow, positive PDM; blue, negative PDM) Scale bars, 10 μm.

treatment, however, induced cav-2 localization in the LLDM (Fig. 4B, lane 5) and reduced association and activation of IR, ERK, and Akt in the HLDM (Fig. 4B, lanes 3 vs. 6). Consequently insulin-induced interaction between cav-2 and IR was attenuated and tyrosine kinase activation of IR were retarded (Fig. 4C). As we investigated effect of actin cytoskeleton disruption on oligomeric status of cav-2, small oligomeric complexes of cav-2 (fractions, 2–4; low MW) were detected in CCD or LatB-treated cells in contrast to large oligomeric complexes of cav-2 found in control cells (Fig. 4D).

To corroborate our findings a PM model system of GPMV was isolated from Hirc-B cells and analyzed (Fig. 5). Cav-2-GFP did not colocalize with CTB-Alexa Fluor® 594 conjugates (a LLDM marker) (Fig. 5, *Panel 1*) while cav-2-mCherry coalesced with flotillin-1-GFP (a HLDM marker) (Fig. 5, panel 2) in the GPMV. MβCD treatment did not alter coalescence of cav-2-mCherry with flotillin-1-GFP (Fig. 5, panel 3). Quantitative analysis confirmed the colocalization (%) of cav-2 with flotillin-1 unaffected by cholesterol depletion. In opposition to the results shown in Fig. 5, panels 1 and 2, cav-2-GFP

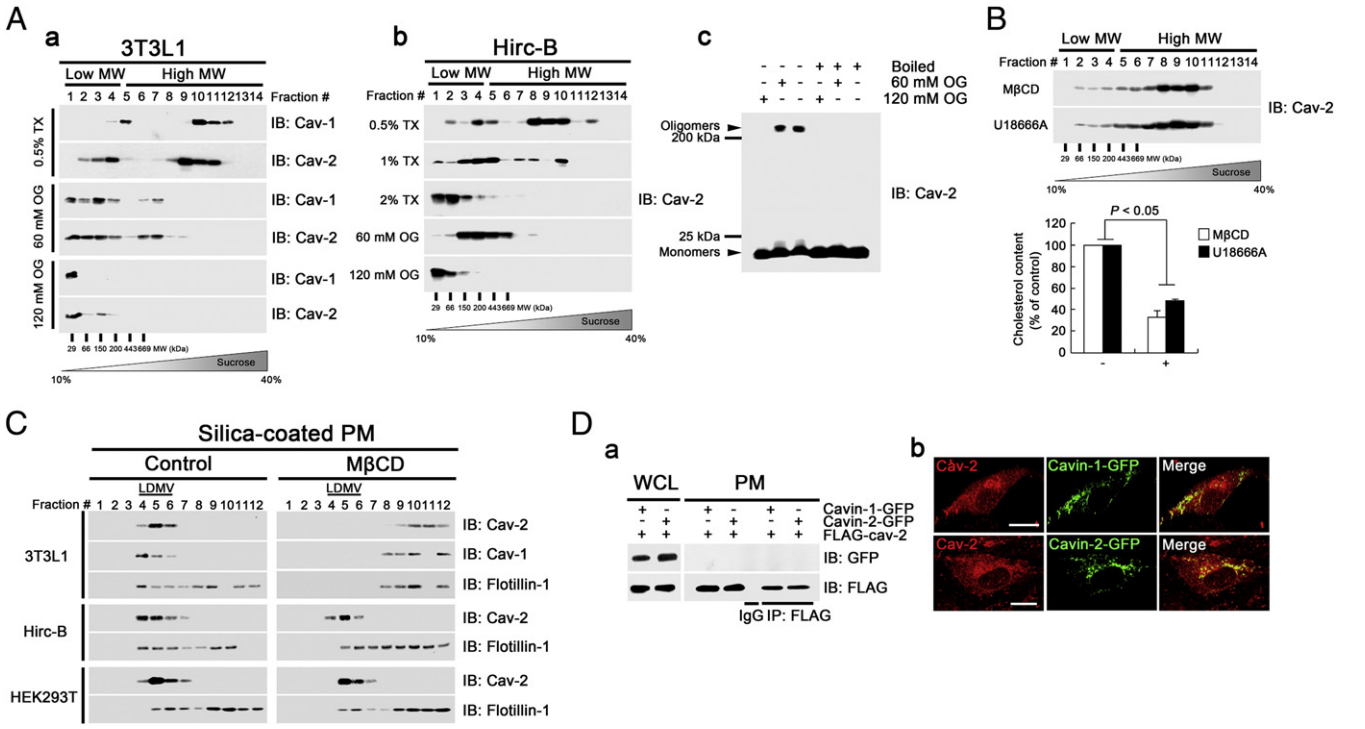

Fig. 3. Homo-oligomeric cav-2 noncaveolar microdomain in the PM is refractory to cholesterol depletion. (A) 3T3L1 (a) or Hirc-B (b) cells were lysed with lysis buffer containing 0.5, 1, and 2% TX-100 or 60 and 120 mM OG as indicated. Whole cell lysates (WCL) were run through 10–40% sucrose velocity gradients. An aliquot of each fraction was resolved by SDS-PAGE and immunoblotted using antibodies against cav-1 and cav-2. (c) Hirc-B cells were lysed with lysis buffer with or without 60 or 120 mM OG. WCL were added with SDS-PAGE loading buffer and boiled or incubated with SDS-PAGE loading buffer excluding β-mercaptoethanol at RT for 30 min and subjected to immunoblotting using antibody against cav-2. (B) Hirc-B cells were treated with or without 10 mM MβCD for 2 h or 20 μg/ml U18666A for 24 h and lysed with lysis buffer containing 0.5% TX-100. WCL were run through 10–40% sucrose velocity gradients. An aliquot of each fraction was resolved by SDS-PAGE and immunoblotted using antibody against cav-2. Cholesterol levels were quantitated using a cholesterol assay kit ($n = 3$, mean ± S.E.). (C) Cells were treated with or without MβCD (3T3L1 and Hirc-B cells, 10 mM for 2 h; cav-2-transfected HEK293T cells, 20 mM for 1 h) and subjected to PM isolation using silica-coating method. The silica-coated PM were sheared by sonication and subjected to sucrose density gradient centrifugation. An aliquot of each fraction was resolved by SDS-PAGE and immunoblotted using antibodies against cav-2, cav-1, and flotillin-1. (D) (a) FLAG-cav-2 and cavin-1-GFP or cavin-2-GFP-cotransfected HEK293T cells were subjected to PM isolation. The purified PM were immunoprecipitated with anti-FLAG antibody and subjected to immunoblot analysis with anti-GFP and anti-FLAG antibodies. (b) Cavin-1-GFP or cavin-2-GFP-transfected Hirc-B cells were labeled with anti-cav-2 antibody followed by TRITC-conjugated antibody. Scale bars, 10 μm.

colocalized with CTB-Alexa Fluor® 594 conjugates (Fig. 5, panel 4) while colocalization of cav-2-mCherry with flotillin-1-GFP was abrogated in the GPMV (Fig. 5, panels 5 and 6) by actin filament disruption. Quantitative analysis verified inhibition in the colocalization (%) of cav-2 with flotillin-1 by CCD or LatB treatment. Taken together, these data show that intact actin cytoskeleton is required for formation of large oligomeric complexes of cav-2 and sustenance of their localization in the HLDM and suggest that homo-oligomeric cav-2 in the PM facilitates IR recruiting and regulates insulin signaling cascade thru activation of IR signaling by direct interaction between cav-2 and IR.

3.5. Reconstitution of functional homo-oligomeric cav-2 microdomain in the PM for IR signaling activation

To explore if absence of cav-2 in the HLDM leads to inhibition of IR signaling activation, cav-2 shRNA stable Hirc-B cells were generated (Fig. 6A). As shown in Fig. 6B, a, in the cav-2 shRNA stable cells, insulin-induced tyrosine kinase activation of IR and phosphorylation of ERK and Akt were not detected in the HLDM. However, ectopic expression of cav-2 restored cav-2 colocalization with IR in the HLDM whereby IR signaling activation was processed in response to insulin (Fig. 6B, b). When effect of cav-2 depletion on IR signaling activation in total cellular level was assessed, cav-2 siRNA significantly attenuated insulin-induced activation of IR, ERK, and Akt (Fig. 6C). These results show that cav-2-enriched microdomain in the PM specifically regulates IR signaling activation. To test whether oligomeric status is important to regulate IR signaling activation in the cav-2-enriched microdomain, FLAG-cav-$2_{\Delta 47-86}$, an oligomerization domain deletion mutant expressing monomeric form of cav-2 (Fig. 6D) was ectopically transfected. The mutant failed to localize to the PM and insulin signaling activation was not processed in the HLDM in the FLAG-cav-$2_{\Delta 47-86}$-transfected cav-2 shRNA stable Hirc-B cells (Fig. 6E). To clarify if the reconstitution of homo-oligomeric cav-2 microdomain in the HLDM triggers IR recruitment to the microdomain, IR level in the HLDM relative to WCL was analyzed in the cav-2 shRNA stable cells. Control cells exhibited reduced IR and ERK and Akt levels in the HLDM as compared to WCL and attenuation in activation of IR and ERK and Akt in response to insulin (Fig. 6F, lanes 1 vs. 3). When cav-2 was reexpressed, IR association with the HLDM was dramatically elevated (Fig. 6F, lane 6) and insulin-induced activation of IR, ERK, and Akt was processed (Fig. 6F, lanes 3 vs. 6). As shown in Fig. 6E, cav-$2_{\Delta 47-86}$ mutant was not detected in the HLDM and its reexpression caused no effect on the IR recruiting and signaling activation in the HLDM (Fig. 6F, lane 9). Thus, these data show that homo-oligomeric form of cav-2 is required for the regulation of IR signaling activation in the HLDM.

3.6. IR signaling activation via reconstituted homo-oligomeric cav-2 noncaveolar microdomain by increasing status of cav-2 expression over cav-1

In 3T3L1 cells having caveolae [42], cholesterol depletion (~80% depletion) by MβCD treatment (Fig. 7A) prevented activation of insulin signaling (Fig. 7, B and C). Whether expression of cav-2 enables to activate IR signaling was tested in MβCD-treated 3T3L1 cells. The

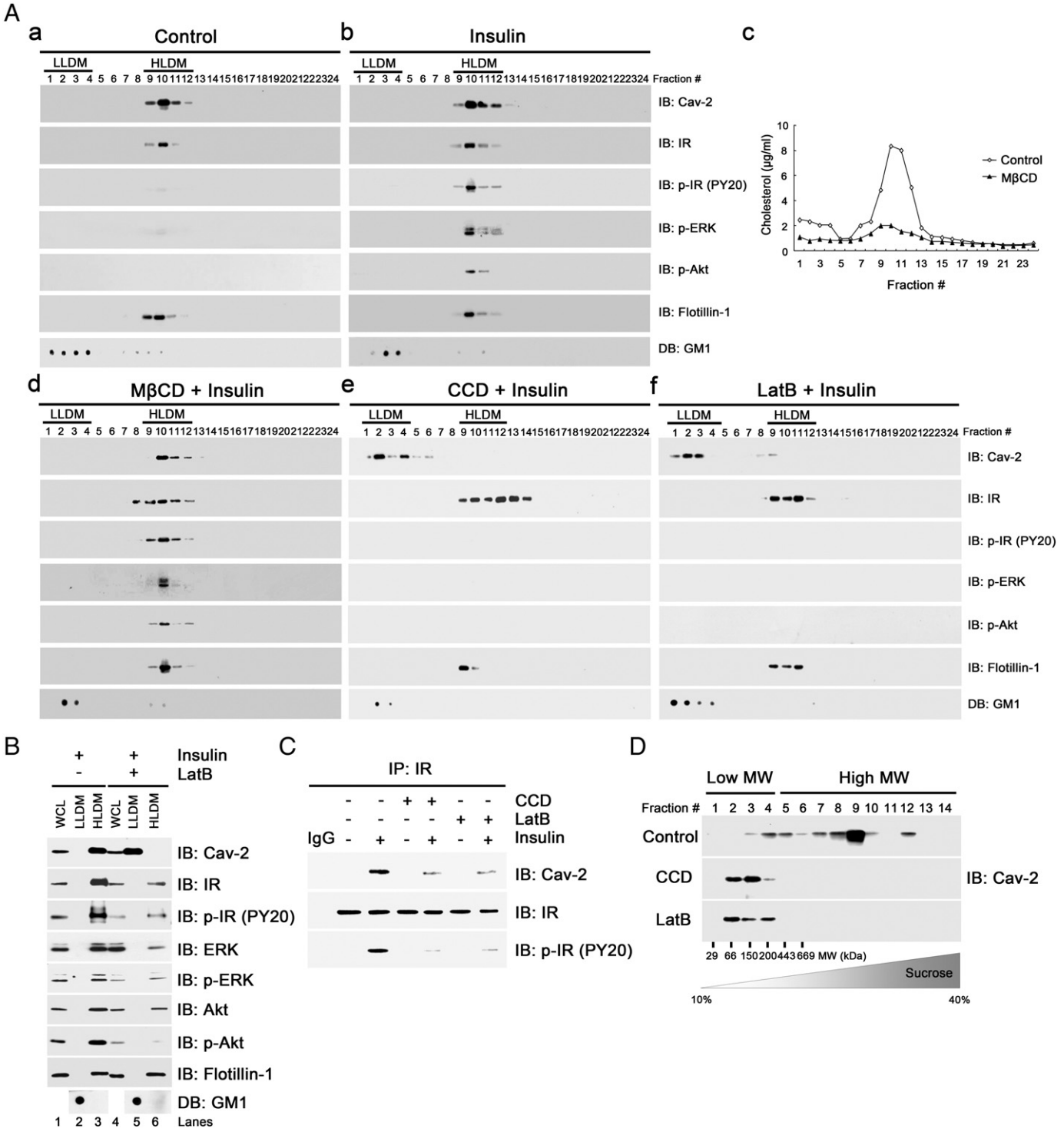

Fig. 4. Actin cytoskeleton is required for sustenance of cav-2 localization and IR signaling activation in the HLDM. (A) Hirc-B cells were treated as follows; untreated control (a), 100 nM insulin for 10 min (b), 10 mM MβCD for 2 h prior to incubation with 100 nM insulin for 10 min (d), 1 μM CCD for 15 min prior to incubation with 100 nM insulin for 10 min (e), 1 μM LatB for 30 min prior to incubation with 100 nM insulin for 10 min (f). The cells were subjected to PM isolation. The purified PM were separated to LLDM and HLDM using four-step sucrose density gradient fractionation. An aliquot of each fraction was resolved by SDS-PAGE and immunoblotted using antibodies against cav-2, IR, PY20, p-ERK, and p-Akt. Each fraction was dot-blotted onto a nitrocellulose membrane to detect ganglioside GM1 with HRP-conjugated CTB. Ganglioside GM1 and flotillin-1 are used for markers for the LLDM and HLDM, respectively. (c) Cholesterol levels were quantitated from an aliquot of each fraction using a cholesterol assay kit. (B) Hirc-B cells were pretreated with or without 1 μM LatB for 30 min followed by incubation with 100 nM insulin for 10 min and subjected to total cell lysis to yield WCL or PM isolation. The purified PM were separated to LLDM and HLDM and fractions 1–4 were combined for LLDM and 9–12 for HLDM fractions. Protein was extracted from the fractions using TCA precipitation and rehydration buffer (7 M urea, 2 M Thiolurea, 4% chaps, and 1 mM PMSF). Equal amounts of protein from WCL and LLDM and HLDM fractions were resolved by SDS-PAGE and immunoblotted using antibodies against cav-2, IR, PY20, ERK, p-ERK, Akt, p-Akt, and flotillin-1. The LLDM and HLDM fractions were dot-blotted onto a nitrocellulose membrane to detect ganglioside GM1 with HRP-conjugated CTB (C) Cells were pretreated with or without 1 μM CCD for 15 min or 1 μM LatB for 30 min followed by incubation with or without 100 nM insulin for 10 min. WCL were immunoprecipitated with anti-IR antibody and subjected to immunoblotting with antibodies against cav-2, IR, and PY20. (D) Cells were treated with or without 1 μM CCD for 15 min or 1 μM LatB for 30 min and lysed with lysis buffer containing 0.5% TX-100. WCL were run through 10–40% sucrose velocity gradients. An aliquot of each fraction was resolved by SDS-PAGE and immunoblotted using antibody against cav-2.

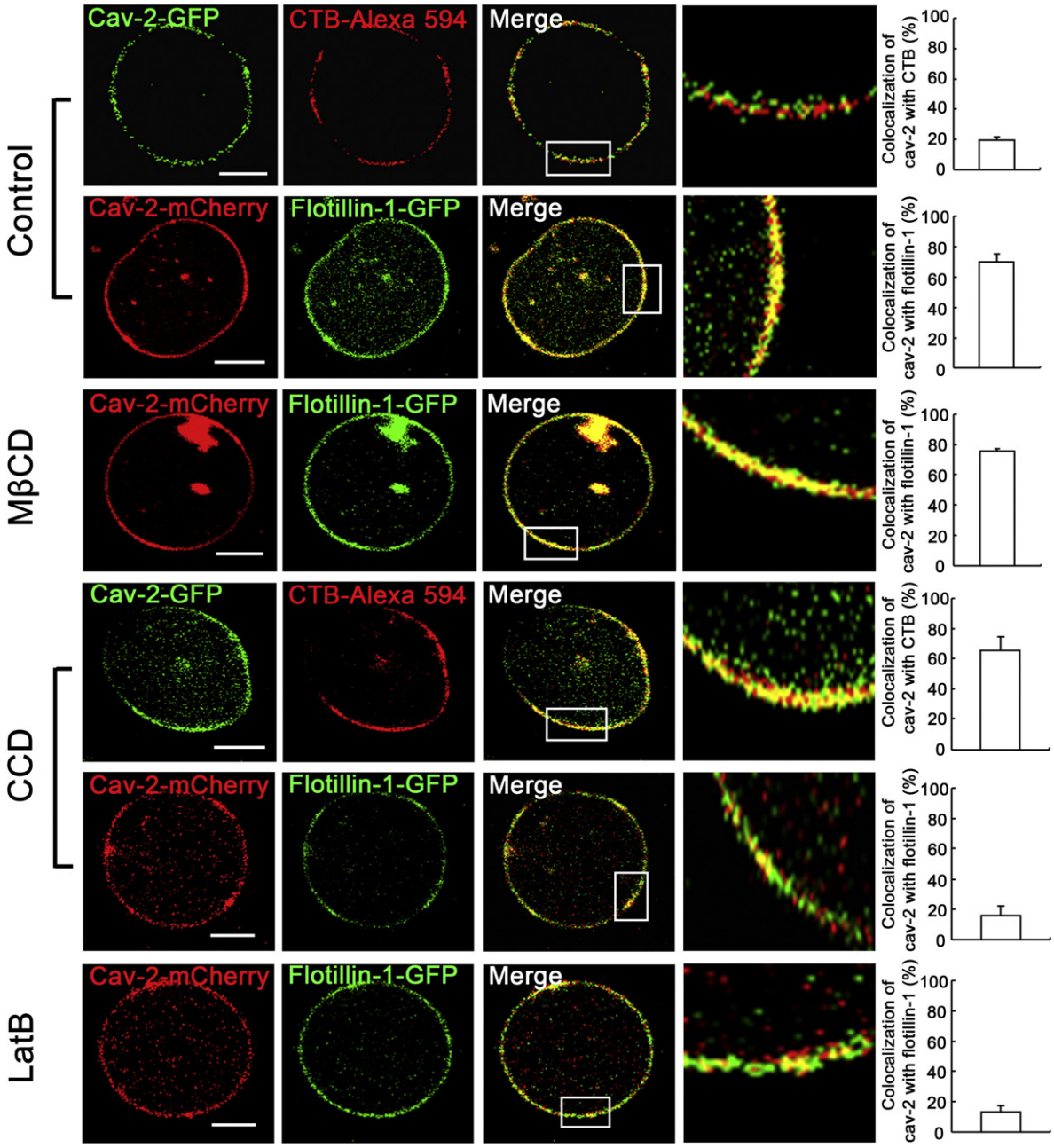

Fig. 5. Colocalization of cav-2 with flotillin-1 in the GPMVs is abrogated by disruption of actin cytoskeleton, but not depletion of cholesterol. Hirc-B cells were transfected with cav-2-GFP or cotransfected with cav-2-mCherry and flotillin-1-GFP. The cells were treated with or without 10 mM MβCD for 2 h, 1 μM CCD for 15 min, or 1 μM LatB for 30 min. GPMVs were isolated from the cells and labeled with 2 μg/ml CTB-Alexa Fluor® 594 conjugates. The colocalization of cav-2-GFP with CTB-Alexa Fluor® 594 conjugates or cav-2-mCherry with flotillin-1-GFP was quantified by the Colocalization Finder Plugin of Image J ($n = 3$, mean ± S.E.). Scale bars, 5 μm.

ectopic cav-2 transfection increased cav-2 expression by ~2.0 fold and decreased ~50% of cav-1 expression as compared to endogenous cav-2 and cav-1 levels, respectively (Fig. 7B, lanes 1–4 vs. 5–8). The reduction of cav-1 and elevation of cav-2 did not alter activation of IR, ERK, and Akt in response to insulin (Fig. 7B, lanes 2 vs. 6). However, insulin signaling retarded by MβCD treatment was restored by the elevation of cav-2 expression (Fig. 7B, lanes 4 vs. 8). When effect of cav-2 expression in cav-1-depleted cells was investigated, cav-1 siRNA decreased ~90% of cav-1 and ~70% of cav-2 protein levels (Fig. 7C, lanes 1–4 vs. 5–8) and attenuated insulin-induced activation of IR, ERK, and Akt (Fig. 7C, lanes 2 vs. 6). MβCD treatment-induced retardation of insulin signaling was aggravated by cav-1 down-regulation (Fig. 7C, lanes 4 vs. 8). Subsequent transfection of cav-2 restoring cav-2 status to the levels of scramble controls and abolishing cav-1 expression (Fig. 7C, lanes 5–8 vs. 9–12) resulted in activation of insulin signaling (Fig. 7C, lanes 6 vs. 10) that was not affected by cholesterol depletion (Fig. 7C, lanes 10 vs. *12*). Finally, we investigated if ectopic cav-2 leads to formation of PM noncaveolar microdomain composed of homo-oligomeric cav-2 for IR signaling activation in 3T3L1 cells. As shown in Fig. 7D, a, endogenous cav-2 colocalized with cav-1 in the HLDM where IR signaling was activated in response to insulin. Cav-1 depletion causing disruption of caveolae led to inhibition of IR signaling activation. Consistent with the results shown in Fig. 7C, cav-1 depletion caused significant reduction of cav-2 expression (Fig. 7D, b). Upon subsequent expression of ectopic cav-2, the cav-2 colocalized with IR and activation of insulin signaling was restored in the HLDM in response to insulin (Fig. 7D, c). As the effect of ectopic cav-2 expression on IR recruitment to the HLDM was

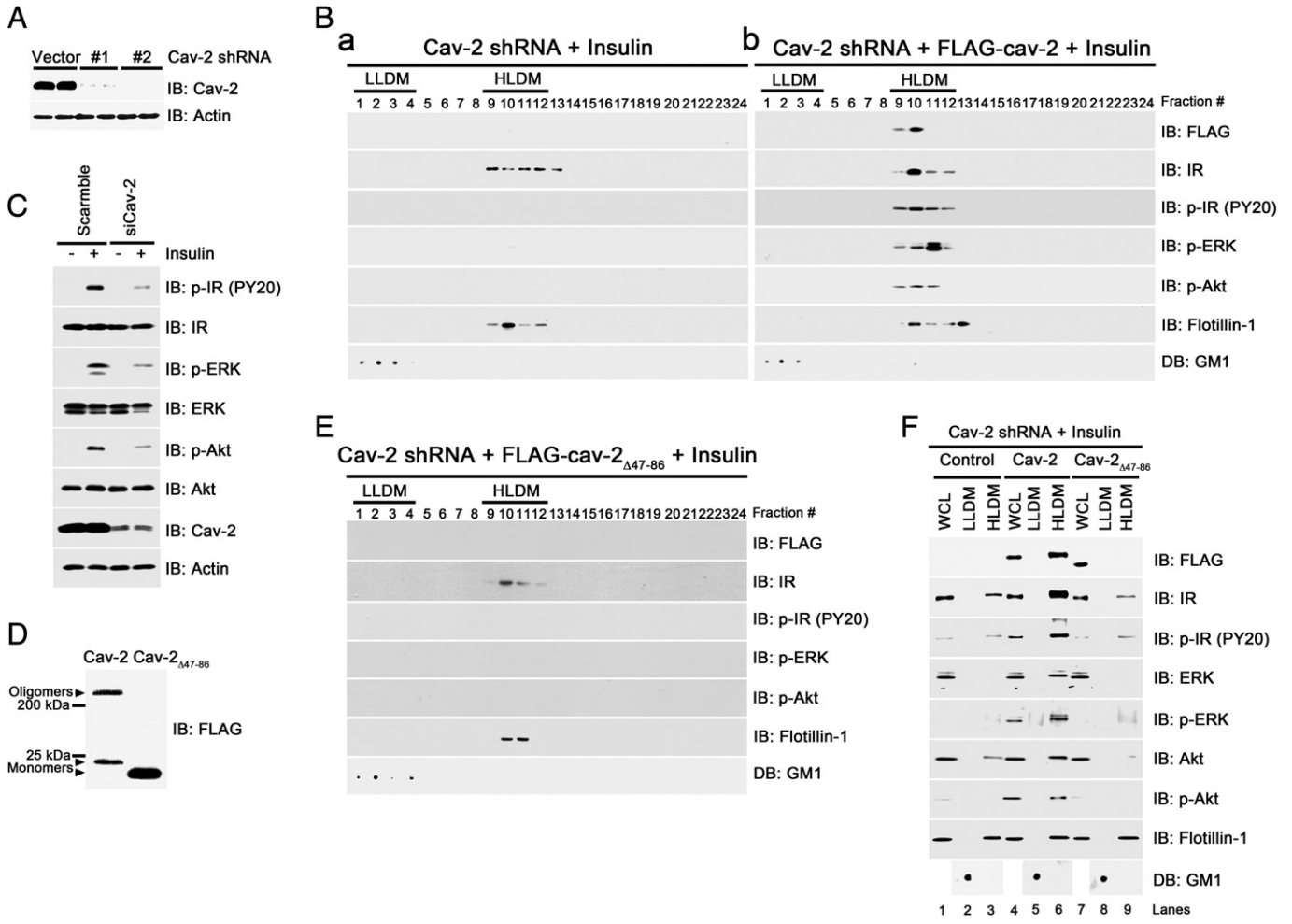

Fig. 6. Formation of functional homo-oligomeric cav-2 in the HLDM is necessary for IR signaling activation. (A) A stable Hirc-B cell line that expresses a cav-2 shRNA (#1 or #2) was generated. The effect of the shRNA on the protein expression of cav-2 is shown by immunoblot analysis. (B) Cav-2 shRNA (#2) stable (a) and FLAG-cav-2-expressed cav-2 shRNA stable (b) Hirc-B cells were treated with 100 nM insulin for 10 min and subjected to PM isolation. The purified PM were separated to LLDM and HLDM and analyzed as in Fig. 4A. (C) Hirc-B cells were transfected with scramble control or cav-2 siRNA and treated with or without 100 nM insulin for 10 min. WCL were subjected to immunoblotting using antibodies against PY20, IR, p-ERK, ERK, p-Akt, Akt, cav-2, and actin. (D) Hirc-B cells were transfected with FLAG-cav-2 or FLAG-cav-$2_{\Delta 47-86}$. WCL were incubated with SDS-PAGE loading buffer excluding β-mercaptoethanol at RT for 30 min and subjected to immunoblotting using antibody against FLAG. (E) FLAG-cav-$2_{\Delta 47-86}$-expressed cav-2 shRNA stable Hirc-B cells were treated with 100 nM insulin for 10 min and subjected to PM isolation. The purified PM were separated to LLDM and HLDM and analyzed as in Fig. 4A. (F) Cav-2 shRNA stable and FLAG-cav-2 or FLAG-cav-$2_{\Delta 47-86}$–expressed cav-2 shRNA stable Hirc-B cells were treated with 100 nM insulin for 10 min and subjected to total cell lysis to yield WCL or PM isolation. The purified PM were separated to LLDM and HLDM and analyzed as in Fig. 4B.

analyzed, IR level in the HLDM relative to WCL was markedly reduced in cav-1-depleted cells as compared to scramble control (Fig. 7E, lanes 3 vs. 6) while cav-2 level was decreased in the HLDM and the WCL as shown in Fig. 7C, lanes 5–8 (Fig. 7E, lanes 1 and 3 vs. 4 and 6). Expression of ectopic cav-2 in the cav-1-depleted cells (Fig. 7E, lanes 4 and 6 vs. 7 and 9) elevated IR, ERK and Akt association in the HLDM (Fig. 7E, lanes 6 vs. 9) and restored insulin-induced tyrosine phosphorylation of IR and activation of ERK and Akt in the HLDM (Fig. 7E, lanes 6 vs. 9). These results demonstrate that IR signaling is transduced via homo-oligomeric cav-2 noncaveolar microdomain in the PM, which is reconstituted by increasing status of cav-2 expression over cav-1.

4. Discussion

IR is localized to and signals via caveolae in adipocytes [47]. Interaction between IR and cav-1 in caveolae leads to an increase in tyrosine kinase activity of IR [48,49]. In liver-derived cells lacking caveolae, however, IR signaling cascade is initiated in noncaveolar raft domains indicating that caveolae and cav-1 is not necessarily required for insulin signaling [50]. Our previous works showed that cav-2 interacts with IR and regulates IR signaling activation in cells lacking cav-1 [21,23]. However, the underlying mechanism for regulation of insulin signaling via the interaction between cav-2 and IR in the PM has not been investigated.

Previous reports showed that cav-2 mainly localized in the Golgi in cells lacking cav-1 and cav-1 expression was required for transport of cav-2 to caveolae in the PM [14,15,18,25–27]. Our recent study also demonstrated that cav-2 exclusively colocalized with GM130 in Hirc-B and HEK293T cells lacking cav-1. But we could not detect PM localization and targeting of cav-2 by fluorescence microscopy even after ectopic expression of cav-1 in the cells, although subcellular fractionation data showed cav-2 localization in the PM [28]. In the present study, cav-2 localization in the PM is demonstrated by confocal immunofluorescence and immunoelectron microscopy (Fig. 1, A, C and D). Further, the PM localization of cav-2 independently of cav-1 is confirmed by a number of independent analyses including subcellular and LDMV fractionation, cell surface biotinylation and PM sheet assays, and GPMV and ectopic reconstitution. Our observation in contrast to the others raises one possibility that cell-type dependent nature could potentially contribute to the different intracellular localization of cav-2. Another possibility would be the technical difficulty to

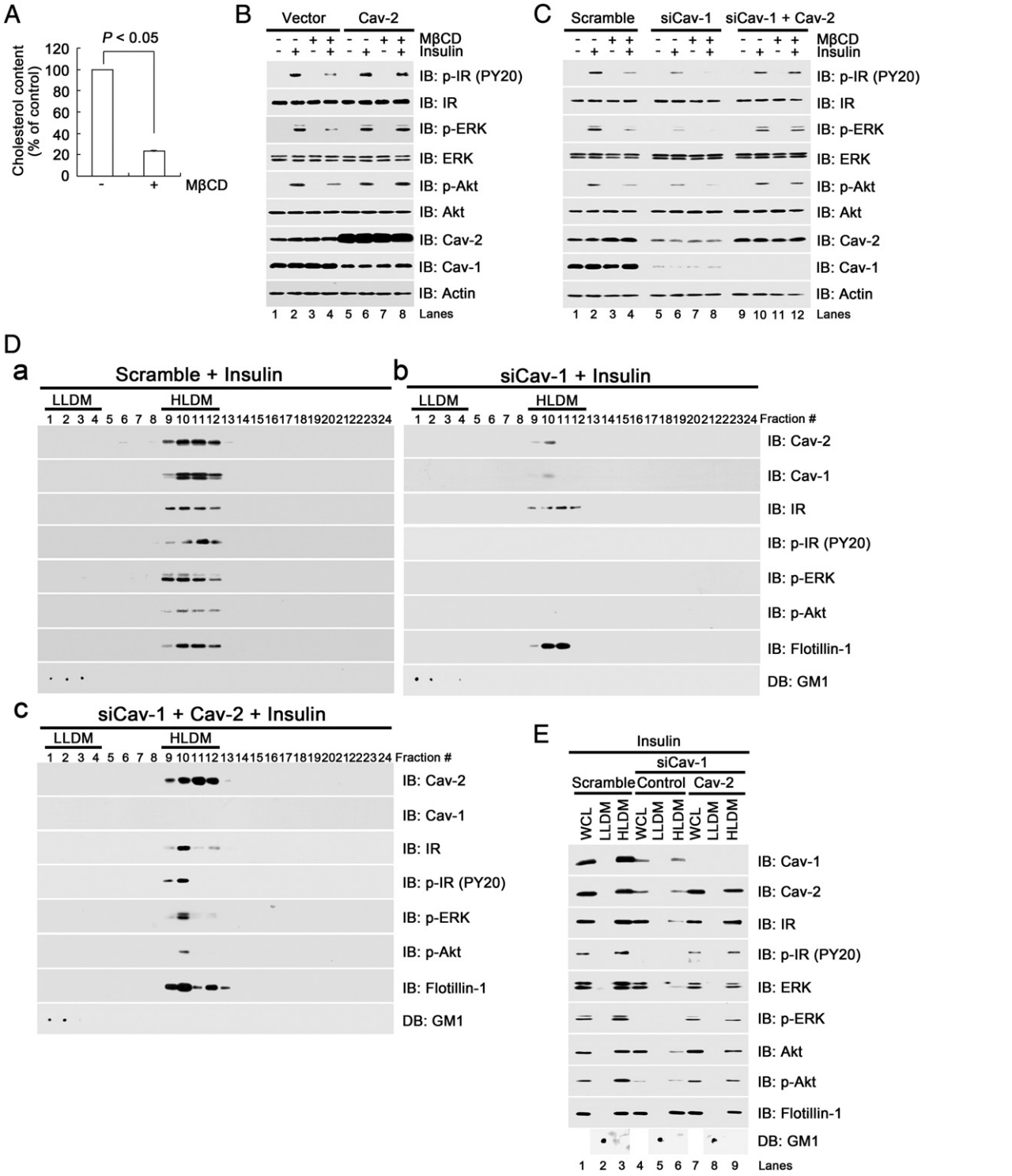

Fig. 7. Elevation of cav-2 expression status relative to cav-1 restores activation of insulin signaling in cholesterol- or/and cav-1-depleted cells. (A) 3T3L1 cells were treated with or without 10 mM MβCD for 2 h. Cholesterol levels were measured by a cholesterol assay kit in the treated cells ($n = 3$, mean ± S.E.). (B and C) 3T3L1 cells were transfected with vector or cav-2 (B), or scramble control, cav-1 siRNA, or cav-1 siRNA and cav-2 (C), and pretreated with or without 10 mM MβCD for 2 h, followed by incubation with or without 100 nM insulin for 10 min. WCL were subjected to immunoblotting using antibodies against PY20, IR, p-ERK, ERK, p-Akt, Akt, cav-2, cav-1, and actin. (D and E) 3T3L1 cells transfected with scramble control (a), cav-1 siRNA (b), or cav-1 siRNA and cav-2 (c) were treated with 100 nM insulin for 10 min and subjected to total cell lysis to yield WCL or PM isolation. The purified PM were separated to LLDM and HLDM and analyzed as in Fig. 4A (D) or Fig. 4B (E).

detect cav-2 alone pool distinctively from either cav-1 alone or cav-1/cav-2 pool in the PM, depending on different cell types because the cav-2-enriched noncaveolar PM microdomains are smaller and dynamic as compared to caveolae which are larger (~200 nm in diameter) and stable structure and can be easily detected by fluorescence and electron microscopy. Although our findings are restricted to three cell types (Hirc-B, HEK293T and 3T3L1 cells), the results suggest that even in the cells constitutively form caveolae in association with cavins in the PM, cav-2 translocates to the PM independently of cav-1 and forms actin cytoskeleton-dependent homooligomerized noncaveolar microdomain with no interaction with cavins in the PM, which is refractory to cholesterol depletion. Further, our findings suggest that

cav-2 localizes in the PM and acts as the major independent functional component for the noncaveolar microdomain or/and as a structural component, as generally described, associated with cav-1 in caveolae, depending on specific cell types.

The present data provide insight into the molecular mechanism responsible for PM targeting of cav-2 in the absence of cav-1. A small GTPase Rab6 regulates exocytic transport by enhancing kinesin, a microtubule-dependent motor protein-driven movement of secretory vesicle from the Golgi [40]. We have shown that cav-2 specifically interacts with Rab6, but not Rab5 and Rab1 [28]. When the cells lacking cav-1, in which cav-2 localizes in the Golgi and PM (Fig. 1) were transfected with Rab6 siRNA or GDP-bound form of Rab6, or treated with colchicine, cav-2 targeting to the PM was greatly retarded (Fig. 2). Thus the present data reveal that Rab6 regulates microtubule-dependent exocytic transport of cav-2 from the Golgi to the PM independently of cav-1.

The present study shows that a functional cav-2-enriched microdomain is present in the PM for insulin signaling. The novel noncaveolar microdomain is composed of homo-oligomeric cav-2, in which IR localizes and its tyrosine kinase activation and phosphorylation of ERK and Akt are processed in response to insulin. Of interest, IR signaling activation in the microdomain was unaffected by perturbation of cholesterol (Fig. 4) and by depletion of ganglioside (Supplementary Fig. 1) or sphingomyelin (Supplementary Fig. 2). However, actin cytoskeleton disruption caused dissipation of cav-2 in the microdomain resulting in no IR recruitment to the microdomain thereby restraining IR activation (Fig. 4). Further actin cytoskeleton-dependent maintenance of large oligomeric form of cav-2 in the microdomain was crucial for cav-2 interaction with IR and subsequent activation of insulin signaling (Figs. 4 and 6). Together, the present data show that a novel cav-2-oligomerized microdomain, which serves as a platform for IR to regulate insulin signaling cascade, exists depending on intact actin cytoskeleton and is distinct from caveolae and cholesterol/sphingolipid-enriched microdomain in the PM.

Actin cytoskeleton disruption facilitated rapid caveolar endocytosis [51,52]. The present data show that depolymerization of actin caused cav-2 depletion in the HLDM and its relocalization in the LLDM in the form of small oligomeric complexes. However no significant reduction of cav-2 level in the LLDM was detected, indicating no facilitative endocytosis of cav-2 (Fig. 4). Our ongoing investigation on the cav-2 endocytosis by using subcellular fractionation has shown that cav-2 in the PM pool is gradually decreased in response to insulin in a time-dependent manner. Although these results suggest that cav-2 internalization occurs in the PM, further work is necessary to identify the precise mechanism for cav-2 endocytosis and actin dependency on oligomerization status of cav-2 in the PM.

When structural feature of cav-2-oligomerized microdomain was assessed by fractionating LDMVs which contain invaginated caveolae protected from shearing of silica-coated PMs (Fig. 3C), cav-2 was detected in the LDMV of 3T3L1 cells having caveolae. Upon MβCD treatment, cav-2 was no longer protected from the shearing, apparently resulted from caveolae disruption. Interestingly, cav-2 was found in the LDMV in cells having no cav-1 and caveolae and cav-2 cofractionated in the LDMV was unaffected by MβCD treatment. These results suggest that cav-2-oligomerized microdomain in the PM exists in a morphologically protected structure against silica shearing of the PM or that a novel caveolae consisted of homo-oligomeric cav-2 is present in the PM. However, electron microscopic analysis showed no morphologically detectable caveolae (Fig. 1C, right panel). Further, cav-2 did not interact with cavin-1 and cavin-2 which are required for caveolae biogenesis [42] in the PM (Fig. 3D). Together, these data suggest that a novel noncaveolar microdomain composed of homo-oligomeric cav-2 with neutral lipids, which are unable to ionic interact with cationic silica exists in the topology of planar shape in the PM and is distinct from the morphologically invaginated omega shape caveolae.

Cav-1-deficient mice showed ~95% reduction of cav-2 protein level and defective IR signaling in adipose tissue [53]. Cav-2-deficient mice exhibited a mild reduction of cav-1 expression and cav-1 localization in caveolae with no change in IR protein level [17,53], suggesting that IR signaling could be processed in caveolae. The present data show that elevation of cav-2 expression promotes IR signaling despite reduction of cav-1 protein level and induces the noncaveolar activation of insulin signaling in caveolae-deficient cells (Fig. 7). Thus, our findings provide a molecular mechanism for regulation of insulin signaling by formation and maintenance of cav-2-enriched noncaveolar microdomain in the PM by modulating status of caveolin expression. It will be interesting to test if defective IR signaling observed in the cav-1-deficient mice can be rescued by increasing status of cav-2 expression.

Acknowledgments

This work was supported by the National Research Foundation of Korea (NRF) grants funded by the Korea government (MEST) (No. 2011-0014898 and No. 2010-0007897) to Y. P. and (No. 2012R1A1A2041550) to H. K. K. J. and D. J. have been supported by scholarship from the BK21 Program (MEST). J. L. is a recipient of the Graduate Research Fellowship from Gyeongsang National University (2010–2012).

Appendix A. Supplementary data

Supplementary data to this article can be found online at http://dx.doi.org/10.1016/j.bbamcr.2013.05.003.

References

[1] K. Simons, E. Ikonen, Functional rafts in cell membranes, Nature 387 (1997) 569–572.
[2] D. Lingwood, K. Simons, Lipid rafts as a membrane-organizing principle, Science 327 (2010) 46–50.
[3] J.F. Hancock, Lipid rafts: contentious only from simplistic standpoints, Nat. Rev. Mol. Cell Biol. 7 (2006) 456–462.
[4] K. Simons, D. Toomre, Lipid rafts and signal transduction, Nat. Rev. Mol. Cell Biol. 1 (2000) 31–39.
[5] C.J. Fielding, P.E. Fielding, Cholesterol and caveolae: structural and functional relationships, Biochim. Biophys. Acta 1529 (2000) 210–222.
[6] E. Ikonen, S. Heino, S. Lusa, Caveolins and membrane cholesterol, Biochem. Soc. Trans. 32 (2004) 121–123.
[7] T. Fujimoto, GPI-anchored proteins, glycosphingolipids, and sphingomyelin are sequestered to caveolae only after crosslinking, J. Histochem. Cytochem. 44 (1996) 929–941.
[8] R.G. Parton, Ultrastructural localization of gangliosides; GM1 is concentrated in caveolae, J. Histochem. Cytochem. 42 (1994) 155–166.
[9] K. Iwabuchi, K. Handa, S. Hakomori, Separation of "glycosphingolipid signaling domain" from caveolin-containing membrane fraction in mouse melanoma B16 cells and its role in cell adhesion coupled with signaling, J. Biol. Chem. 273 (1998) 33766–33773.
[10] K. Iwabuchi, Y. Zhang, K. Handa, D.A. Withers, P. Sinaÿ, S. Hakomori, Reconstitution of membranes simulating "glycosignaling domain" and their susceptibility to lyso-GM3, J. Biol. Chem. 275 (2000) 15174–15181.
[11] S.B. Gaudreault, J.F. Blain, J.P. Gratton, J. Poirier, A role for caveolin-1 in post-injury reactive neuronal plasticity, J. Neurochem. 92 (2005) 831–839.
[12] J. Harris, D. Werling, M. Koss, P. Monaghan, G. Taylor, C.J. Howard, Expression of caveolin by bovine lymphocytes and antigen-presenting cells, Immunology 105 (2002) 190–195.
[13] B.P. Head, P.A. Insel, Do caveolins regulate cells by actions outside of caveolae? Trends Cell Biol. 17 (2007) 51–57.
[14] R. Mora, V.L. Bonilha, A. Marmorstein, P.E. Scherer, D. Brown, M.P. Lisanti, E. Rodriguez-Boulan, Caveolin-2 localizes to the golgi complex but redistributes to plasma membrane, caveolae, and rafts when co-expressed with caveolin-1, J. Biol. Chem. 274 (1999) 25708–25717.
[15] L. Breuza, S. Corby, J.P. Arsanto, M.H. Delgrossi, P. Scheiffele, A. Le Bivic, The scaffolding domain of caveolin 2 is responsible for its Golgi localization in Caco-2 cells, J. Cell Sci. 115 (2002) 4457–4467.
[16] D. Volonte, F. Galbiati, S. Li, K. Nishiyama, T. Okamoto, M.P. Lisanti, Flotillins/cavatellins are differentially expressed in cells and tissues and form a hetero-oligomeric complex with caveolins in vivo. Characterization and epitope-mapping of a novel flotillin-1 monoclonal antibody probe, J. Biol. Chem. 274 (1999) 12702–12709.

[17] B. Razani, X.B. Wang, J.A. Engelman, M. Battista, G. Lagaud, X.L. Zhang, B. Kneitz, H. Hou Jr., G.J. Christ, W. Edelmann, M.P. Lisanti, Caveolin-2-deficient mice show evidence of severe pulmonary dysfunction without disruption of caveolae, Mol. Cell Biol. 22 (2002) 2329–2344.
[18] U. Lahtinen, M. Honsho, R.G. Parton, K. Simons, P. Verkade, Involvement of caveolin-2 in caveolar biogenesis in MDCK cells, FEBS Lett. 538 (2003) 85–88.
[19] P. Lajoie, J.G. Goetz, J.W. Dennis, I.R. Nabi, Lattices, rafts, and scaffolds: domain regulation of receptor signaling at the plasma membrane, J. Cell Biol. 185 (2009) 381–385.
[20] S. Kim, Y. Pak, Caveolin-2 regulation of the cell cycle in response to insulin in Hirc-B fibroblast cells, Biochem. Biophys. Res. Commun. 330 (2005) 88–96.
[21] H. Kwon, K. Jeong, Y. Pak, Identification of pY19-caveolin-2 as a positive regulator of insulin-stimulated actin cytoskeleton-dependent mitogenesis, J. Cell. Mol. Med. 13 (2009) 1549–1564.
[22] H. Kwon, K. Jeong, E.M. Hwang, J.Y. Park, S.G. Hong, W.S. Choi, Y. Pak, Caveolin-2 regulation of STAT3 transcriptional activation in response to insulin, Biochim. Biophys. Acta 1793 (2009) 1325–1333.
[23] H. Kwon, Y. Pak, Prolonged tyrosine kinase activation of insulin receptor by pY27-caveolin-2, Biochem. Biophys. Res. Commun. 391 (2010) 49–55.
[24] H. Kwon, K. Jeong, E.M. Hwang, J.Y. Park, Y. Pak, A novel domain of caveolin-2 that controls nuclear targeting: regulation of insulin-specific ERK activation and nuclear translocation by caveolin-2, J. Cell. Mol. Med. 15 (2011) 888–908.
[25] I. Parolini, M. Sargiacomo, F. Galbiati, G. Rizzo, F. Grignani, J.A. Engelman, T. Okamoto, T. Ikezu, P.E. Scherer, R. Mora, E. Rodriguez-Boulan, C. Peschle, M.P. Lisanti, Expression of caveolin-1 is required for the transport of caveolin-2 to the plasma membrane: retention of caveolin-2 at the level of the golgi complex, J. Biol. Chem. 274 (1999) 25718–25725.
[26] A. Manninen, P. Verkade, S. Le Lay, J. Torkko, M. Kasper, J. Füllekrug, K. Simons, Caveolin-1 is not essential for biosynthetic apical membrane transport, Mol. Cell Biol. 25 (2005) 10087–10096.
[27] B. Razani, J.A. Engelman, X.B. Wang, W. Schubert, X.L. Zhang, C.B. Marks, F. Macaluso, R.G. Russell, M. Li, R.G. Pestell, D. Di Vizio, H. Hou Jr., B. Kneitz, G. Lagaud, G.J. Christ, W. Edelmann, M.P. Lisanti, Caveolin-1 null mice are viable but show evidence of hyperproliferative and vascular abnormalities, J. Biol. Chem. 276 (2001) 38121–38138.
[28] K. Jeong, H. Kwon, J. Lee, D. Jang, E.M. Hwang, J.Y. Park, Y. Pak, Rab6-mediated retrograde transport regulates inner nuclear membrane targeting of caveolin-2 in response to insulin, Traffic 13 (2012) 1218–1233.
[29] I.A. Simpson, D.R. Yver, P.J. Hissin, L.J. Wardzala, E. Karnieli, L.B. Salans, S.W. Cushman, Insulin-stimulated translocation of glucose transporters in the isolated rat adipose cells: characterization of subcellular fractions, Biochim. Biophys. Acta 763 (1983) 393–407.
[30] R.C. Piper, L.J. Hess, D.E. James, Differential sorting of two glucose transporters expressed in insulin-sensitive cells, Am. J. Physiol. 260 (1991) C570–C580.
[31] Q. Li, A. Lau, T.J. Morris, L. Guo, C.B. Fordyce, E.F. Stanley, A syntaxin 1, Galpha(o), and N-type calcium channel complex at a presynaptic nerve terminal: analysis by quantitative immunocolocalization, J. Neurosci. 24 (2004) 4070–4081.
[32] N. Benlimame, P.U. Le, I.R. Nabi, Localization of autocrine motility factor receptor to caveolae and clathrin-independent internalization of its ligand to smooth endoplasmic reticulum, Mol. Biol. Cell 9 (1998) 1773–1786.
[33] A. Hayer, M. Stoeber, C. Bissig, A. Helenius, Biogenesis of caveolae: stepwise assembly of large caveolin and cavin complexes, Traffic 11 (2010) 361–382.
[34] A. Hayer, M. Stoeber, D. Ritz, S. Engel, H.H. Meyer, A. Helenius, Caveolin-1 is ubiquitinated and targeted to intralumenal vesicles in endolysosomes for degradation, J. Cell Biol. 191 (2010) 615–629.
[35] X. Li, Q. Jin, J. Cao, C. Xie, R. Cao, Z. Liu, J. Xiong, J. Li, X. Yang, P. Chen, S. Liang, Evaluation of two cell surface modification methods for proteomic analysis of plasma membrane from isolated mouse hepatocytes, Biochim. Biophys. Acta 1794 (2009) 32–41.
[36] K.S. Song, S. Li, T. Okamoto, L.A. Quilliam, M. Sargiacomo, M.P. Lisanti, Co-purification and direct interaction of Ras with caveolin, an integral membrane protein of caveolae microdomain: detergent-free purification of caveolae microdomains, J. Biol. Chem. 271 (1996) 9690–9697.
[37] Y. Yao, S. Hong, H. Zhou, T. Yuan, R. Zeng, K. Liao, The differential protein and lipid compositions of noncaveolar lipid microdomains and caveolae, Cell Res. 19 (2009) 497–506.
[38] L. Ge, W. Qi, L.J. Wang, H.H. Miao, Y.X. Qu, B.L. Li, B.L. Song, Flotillins play an essential role in Niemann-Pick C1-like 1-mediated cholesterol uptake, Proc. Natl. Acad. Sci. U. S. A. 108 (2011) 551–556.
[39] T. Baumgart, A.T. Hammond, P. Sengupta, S.T. Hess, D.A. Holowka, B.A. Baird, W.W. Webb, Large-scale fluid/fluid phase separation of proteins and lipids in giant plasma membrane vesicles, Proc. Natl. Acad. Sci. U. S. A. 104 (2007) 3165–3170.
[40] I. Grigoriev, D. Splinter, N. Keijzer, P.S. Wulf, J. Demmers, T. Ohtsuka, M. Modesti, I.V. Maly, F. Grosveld, C.C. Hoogenraad, A. Akhmanova, Rab6 regulates transport and targeting of exocytotic carriers, Dev. Cell 13 (2007) 305–314.
[41] L. Cubells, S. Vilà de Muga, F. Tebar, P. Wood, R. Evans, M. Ingelmo-Torres, M. Calvo, K. Gaus, A. Pol, T. Grewal, C. Enrich, Annexin A6-induced alterations in cholesterol transport and caveolin export from the Golgi complex, Traffic 8 (2007) 1568–1589.
[42] P.E. Scherer, R.Y. Lewis, D. Volonte, J.A. Engelman, F. Galbiati, J. Couet, D.S. Kohtz, E. van Donselaar, P. Peters, M.P. Lisanti, Cell-type and tissue-specific expression of caveolin-2: caveolins 1 and 2 co-localize and form a stable hetero-oligomeric complex in vivo, J. Biol. Chem. 272 (1997) 29337–29346.
[43] I.R. Nabi, Cavin fever: regulating caveolae, Nat. Cell Biol. 11 (2009) 789–791.
[44] A.R. Saltiel, J.E. Pessin, Insulin signaling in microdomains of the plasma membrane, Traffic 4 (2003) 711–716.
[45] L. JeBailey, A. Rudich, X. Huang, C. Di Ciano-Oliveira, A. Kapus, A. Klip, Skeletal muscle cells and adipocytes differ in their reliance on TC10 and Rac for insulin-induced actin remodeling, Mol. Endocrinol. 18 (2004) 359–372.
[46] M. Barda-Saad, A. Braiman, R. Titerence, S.C. Bunnell, V.A. Barr, L.E. Samelson, Dynamic molecular interactions linking the T cell antigen receptor to the actin cytoskeleton, Nat. Immunol. 6 (2005) 80–89.
[47] J. Gustavsson, S. Parpal, M. Karlsson, C. Ramsing, H. Thorn, M. Borg, M. Lindroth, K.H. Peterson, K.E. Magnusson, P. Strålfors, Localization of the insulin receptor in caveolae of adipocyte plasma membrane, FASEB J. 13 (1999) 1961–1971.
[48] M. Yamamoto, Y. Toya, C. Schwencke, M.P. Lisanti, M.G. Myers Jr., Y. Ishikawa, Caveolin is an activator of insulin receptor signaling, J. Biol. Chem. 273 (1998) 26962–26968.
[49] F.H. Nystrom, H. Chen, L.N. Cong, Y. Li, M.J. Quon, Caveolin-1 interacts with the insulin receptor and can differentially modulate insulin signaling in transfected Cos-7 cells and rat adipose cells, Mol. Endocrinol. 13 (1999) 2013–2024.
[50] S. Vainio, S. Heino, J.E. Mansson, P. Fredman, E. Kuismanen, O. Vaarala, E. Ikonen, Dynamic association of human insulin receptor with lipid rafts in cells lacking caveolae, EMBO Rep. 3 (2002) 95–100.
[51] D.I. Mundy, T. Machleidt, Y.S. Ying, R.G. Anderson, G.S. Bloom, Dual control of caveolar membrane traffic by microtubules and the actin cytoskeleton, J. Cell Sci. 115 (2002) 4327–4339.
[52] L. Pelkmans, D. Püntener, A. Helenius, Local actin polymerization and dynamin recruitment in SV40-induced internalization of caveolae, Science 296 (2002) 535–539.
[53] A.W. Cohen, B. Razani, X.B. Wang, T.P. Combs, T.M. Williams, P.E. Scherer, M.P. Lisanti, Caveolin-1-deficient mice show insulin resistance and defective insulin receptor protein expression in adipose tissue, Am. J. Physiol. Cell Physiol. 285 (2003) C222–C235.